Macromolecules

Article

Cite This: Macromolecules 2018, 51, 1232−1241

Self-Dynamics and Collective Swap-Driven Dynamics in a Particle Model for Vitrimers

Lorenzo Rovigatti,*[,†,‡] Giovanni Nava,[§] Tommaso Bellini,[§] and Francesco Sciortino[‡]

[†]CNR-ISC, Uos Sapienza, Piazzale A. Moro 2, 00185 Roma, Italy

[‡]Department of Physics, Sapienza, Universitá di Roma, Piazzale Aldo Moro 2, I-00185, Roma, Italy

[§]Department of Medical Biotechnology and Translational Medicine, Universita degli Studi di Milano, via Fratelli Cervi 93, I-20090 Segrate, MI, Italy

ABSTRACT: We numerically investigate the self-dynamics and collective dynamics of a simple model for vitrimers—polymeric covalent networks that have the ability to dynamically rearrange the bond structure via exchange reactions, preserving the total connectivity. Specifically, we study a binary mixture of tetrafunctional and bifunctional particles by means of molecular dynamics simulations that naturally incorporate the bond-swapping mechanism. We specifically focus on the dynamics at small wavevector q by simulating 800 000 particles. We observe two distinct collective relaxation processes: (i) a fast vibrational damped mode and (ii) a slow network restructuring dynamics. Unexpectedly, the slow process is characterized by a wavevector-independent (q^0) mode originating from the swap motion of the bonds.

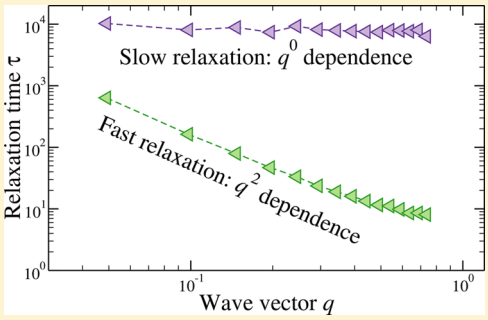

Vitrimers[1−3] are a new class of polymeric materials in which the network nodes, despite the covalent bonding, can change their bonded partners via reversible exchange reactions with unreacted sites. The ability to dynamically rearrange the network structure and the external control (for example, via temperature) of the rate of exchange opens up the possibility to spontaneously heal internal fractures, recycle the material shape, and release applied stresses. Vitrimers significantly differ from thermoplastics and elastomers. Thermoplastics are made by melt of polymers which can be multiply reshaped but are formally soluble. Elastomers are polymers cross-linked via irreversible bonds, and hence the topology of the resulting network is permanent, preventing the possibility to reshape them. Vitrimers are instead characterized by a controllable viscosity and can in principle flow under applied stress if the exchange reaction is sufficiently active. In vitrimers the viscosity is controlled by the presence of a catalyst,[1,4,5] whose efficiency follows an Arrhenius temperature dependence, resulting in a strong-glass-former behavior in Angell's classification.[6]

To grasp the basic feature of a vitrimer system, consider a mixture of two different macromolecules, indicated as A and B in the following (Figure 1). Particle A has f_A bonding sites and particle B f_B. Only sites on unlike particles can bind to each other, forming a covalent bond, e.g., a bond significantly stronger than the thermal energy k_BT. Under these conditions, after mixing the A and B particles the bonding reaction quickly proceeds until all possible bonds are formed. Selecting a nonstoichiometric mixture, i.e., $f_AN_A \neq f_BN_B$, where N_A (N_B) is the number of particles of type A (B), when the reaction is completed, the system is composed by a network of AB bonds with a fixed number of unreacted sites of the majority species (Figure 1a,c). When the thermal vibration of the network brings one of these unreacted sites close to an existing AB bond, an exchange reaction[1,2,7,8] takes place, locally rearranging the network topology. The total number of bonds in the system (and hence the system potential energy) before and after the swap process remains unchanged. Since the total number of bonds is conserved, the dynamics in a vitrimer system can be considered as a stroll on the flat ground state potential energy surface. In time, the system explores all possible maximally bonded configurations such that the maximization of entropy (and only entropy) controls the evolution of the system toward the lowest free-energy state.

The physics of vitrimers is possibly also shared by physical gels well beyond the percolation threshold, when the gel consists of a single almost fully bonded cluster.[9−12] Under these conditions, the thermal energy is sufficiently smaller than the bond energy, and the dynamic evolution is controlled by the activated process of bond breaking and re-forming. Only if a nearby broken bond is present can one of the two newly formed defects rebind, thus contributing to the reconfiguration of the network in a different bonding pattern. Differently from vitrimers, it is the same energy scale of the bond that controls the swapping rate. Gels of DNA nanostars with controlled functionality[13−16] constitute a very appropriate example of physical gels with strong binding energies.

In the past years, a small number of theoretical/numerical investigations of these new materials have appeared. The

Received: October 12, 2017
Revised: December 20, 2017
Published: January 12, 2018

DOI: 10.1021/acs.macromol.7b02186
Macromolecules 2018, 51, 1232−1241

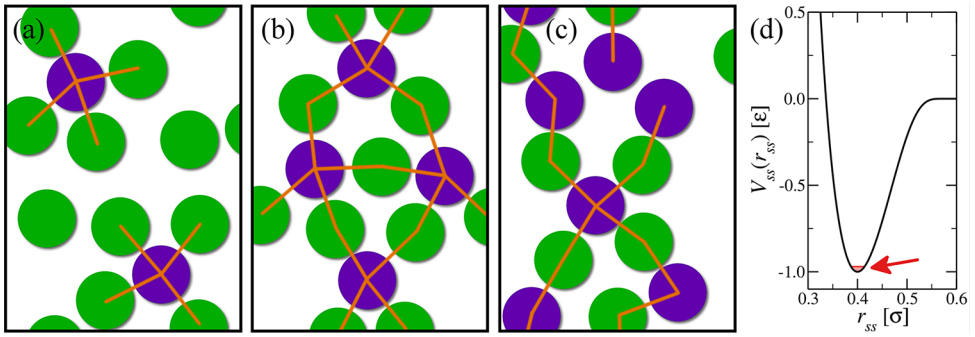

Figure 1. Sketch of systems with (a) an excess of (bifunctional) *B* particles (in green, the case considered in this work), (b) a stoichiometric mixture, and (c) an excess of (tetrafunctional) *A* particles (in violet). Interparticle bonds are depicted as orange straight lines. (d) The site−site interaction potential $V_{ss}(r_{ss})$ (eq 2). The red shaded region pointed out with the arrow gives an idea of the extent of the thermal fluctuations associated with the value of the temperature used in simulations, $k_BT = 0.03$.

thermodynamics of vitrimers has been investigated at particle level by modeling the system as a binary mixture of patchy particles[17] for which the thermodynamic perturbation theory introduced by Wertheim[18,19] can be analytically solved. Theory and associated numerical simulations have provided evidence that under dilution vitrimers do not dissolve. The system progressively expels the majority component, evolving toward the stochiometric relative concentration. The dynamics of the system has been discussed either via a continuum model focusing on the macroscopic viscoelastic properties of the network[20,21] as well as via patchy particle models[17] in which the exchange rate (controlled in real materials by the concentration of catalyst and by the temperature) was treated as an external parameter.

In this article we exploit the recently proposed swap algorithm[22] to perform molecular dynamics simulations of a binary mixture of *A* and *B* particles for different values of the relative concentration, close to the stoichiometric value. We investigate an 800 000-particle system to access the small wavevector q region and make contact with the typical wavelength of light scattering experiments. We focus on the self-dynamics and collective dynamics as a function of q. While the self-dynamics is properly described by a q^{-2} law, we discover a remarkable q-independent (q^0) collective slow relaxation time. This peculiar q dependence, to our knowledge never previously observed in a numerical study of interacting particles, is consistent with what has been recently measured in gels of DNA tetrafunctional nanostars and modeled via a bead−spring model.[23] This behavior has also been observed in systems of microemulsion droplets in solution with telechelic polymers, where the polymers ends preferentially explore the interior of the microemulsion droplets effectively providing a transient link between them.[24] Finally, we offer an explanation of the q^0 collective mode in terms of diffusive motion of the network defects which provides the mechanism for allowing the network to explore all possible bonding configurations, providing a realization of the fluctuating elasticity concept proposed in ref 23.

MODEL AND NUMERICAL METHODS

The model we select is a continuous version of the patchy particle model proposed in ref 17. The system is composed by N_A tetrafunctional ($f_A = 4$) particles and N_B ($f_B = 2$) bifunctional particles, with the fraction of *A* particles indicated as $x \equiv N_A/(N_A + N_B)$. The four interacting sites of *A* particles are arranged in tetrahedral geometry, while the two sites of *B* particles are arranged in polar geometry. When $N_Af_A = N_Bf_B$ (i.e., when $x = x_{fb} \equiv \frac{f_B}{f_A + f_B} = 1/3$), the system at low temperature forms a fully bonded network. When $x \leq x_{fb}$ at low temperature all *A* sites are bonded (and hence p_A, the probability of finding an *A* site bonded, is unity), but there is a finite fraction of unpaired *B* sites. As a result, the probability of finding a bonded *B* site, p_B, is less than unity. More precisely, when all possible bonds are formed (and $x < x_{fb}$)

$$p_B = \frac{f_A N_A}{f_B N_B} = \frac{f_A x}{f_B(1-x)} < 1$$

Hence, there is a finite number of unreacted *B* sites equal to $N_Bf_B(1 - p_B)$, or equivalently $(f_A + f_B)(N_A + N_B)(x_{fb} - x)$. Similarly, the number of unreacted *B* particles (e.g., in monomeric state) is $N_B(1 - p_B)^2$.[9] In the simulation we keep constant $N = 800\,000$ and vary x from 0.3 to $x_{fb} = 1/3$. Table 1 reports some information on the explored states. We note that the percolation threshold (e.g., the presence of an infinite cluster in the system) evaluated according to Flory−Stockmayer arguments[25] is $p_Ap_B = \frac{1}{f_A - 1}$ corresponding to $x_{perc} = 1/7$. All samples studied here are thus well beyond percolation.

Table 1. List of the Investigated Binary Systems[a]

$x \equiv N_A/N$	no. of unreacted *B* sites	p_B	*B* monomers
0.300	160000	0.857	11450
0.320	64000	0.941	1893
0.325	40000	0.963	739
0.330	16000	0.985	121
0.332	6400	0.994	19
0.3325	4000	0.996	8.5
0.333	1600	0.998	2
1/3	0	1.000	0

[a]The table shows the relative composition $x \equiv N_A/N$, the number of unreacted *B* sites (all *A* sites are bonded), acting as swapping sites, the probability p_B that a *B* site is bonded, and finally the number of unbonded *B* monomers. The total number of particles is in all cases $N = 800\,000$.

The volume is fixed to 128.16^3 (in unit of the particle diameter σ), corresponding to a total number density $\rho\sigma^3 = 0.38$. Interactions between the centers of mass of *AA*, *AB*, and *BB* particles are modeled via a repulsive WCA potential[26]

DOI: 10.1021/acs.macromol.7b02186
Macromolecules 2018, 51, 1232−1241

$$V(r) = \begin{cases} 4\epsilon\left[\left(\frac{\sigma}{r}\right)^{12} - \left(\frac{\sigma}{r}\right)^{6}\right] + \epsilon & \text{for } r \le 2^{1/6}\sigma \\ 0 & \text{for } r > 2^{1/6}\sigma \end{cases} \quad (1)$$

The attractive site−site interaction V_{ss} is active only between distinct A and B pairs, it is a function of the site−site distance r_{ss}, and it is modeled through the following function, inspired by the Stillinger−Weber potential[27]

$$V_{ss}(r_{ss}) = \begin{cases} 2\epsilon\left(\frac{\sigma_{ss}^{4}}{2r_{ss}^{4}} - 1\right)e^{\sigma_{ss}/(r_{ss}-r_c)+2} & \text{for } r_{ss} \le r_c \\ 0 & \text{for } r_{ss} > r_c \end{cases} \quad (2)$$

which encodes a short-range attraction (see Figure 1d). Here σ_{ss} controls the position of the minimum of the attractive well (of depth ϵ) and r_c is such that $V_{ss}(r_c) = 0$. We set $\sigma_{ss} = 0.4\sigma$ and $r_c = 1.5\sigma_{ss}$. To implement the single bond per site condition and the swapping mechanism, we encode the method proposed in ref 22. A detailed description of the method can be found in the Appendix. Here we outline the idea behind the algorithm. It consists in adding a repulsive three-body potential acting on all triplets of bonded sites (*ABA* or *BAB*). If a free B site moves close to an existing AB bond, the additional energetic gain associated with the formation of an extra bond is compensated by an energetic loss of tunable strength arising from the three-body potential. As discussed at length in the Appendix, the activation energy for swapping is $(\lambda - 1)\epsilon$, being $\lambda \ge 1$ a model parameter. Hence, it is possible to tune it from a condition of vanishing activation energy up to any barrier height. Since the thermal energy of the simulation is significantly smaller than ϵ, no spontaneous bond-breaking processes are observed. Hence, the system dynamics can be described as a restructuring of the bonds made possible by the swap process. In this condition, the presence of an activation energy only affects the speed of the network restructuring, effectively rescaling the dynamics by an Arrhenius factor dependent on the ratio between the barrier activation energy and ϵ. Since we are interested in understanding how the bond swapping affects the dynamics of the system, we choose to simulate a system where the swap dynamics is fastest. That is when there is no significant energy cost in swapping the bond ($\lambda = 1$, see Appendix). Under these conditions, the time scale of the bond process is entirely controlled by the stoichiometry of the network.

Mass is measured in unit of the particle mass m, energy is measure in unit of ϵ, and k_BT is also measured in unit of ϵ, where k_B is the Boltzmann constant. Distances are measured in unit of σ, and time is measured in units of $t_0 \equiv \sqrt{m\sigma^2/k_BT}$. The equations of motion are integrated with the velocity-Verlet algorithm with a time step $\delta t = 0.003$. We initially employ a modified Andersen thermostat[28] to equilibrate all systems at $k_BT = 0.03$. We then perform production runs in the *NVE* ensemble. The specific value of T is irrelevant as far as it is significantly smaller than ϵ to guarantee that bonds do not thermally break over the course of the simulation. Since we select $x < x_{fb}$, all A sites are always involved in bonds and hence cannot initiate swapping processes. The only possible network reconfiguring events are thus bond swaps where a free B site reacts with a AB bonded pair replacing the B in the bond.

STRUCTURE

To appropriately frame the dynamic information in Fourier space, we show in Figure 2, the partial components of the

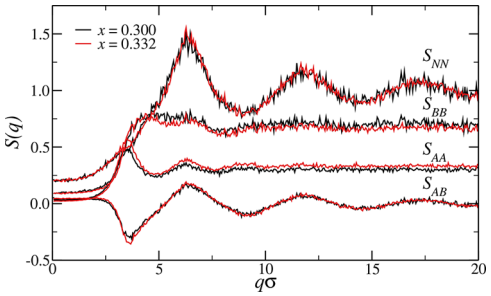

Figure 2. Total (S_{NN}) and partial (S_{AA}, S_{BB}, S_{AB}) structure factors for the $x = 0.300$ (black) and $x = 0.332$ (red) systems.

structure factor S_{AA}, S_{AB}, and S_{BB}, and the total $S_{NN} = xS_{AA} + (1 - x)S_{BB} + 2[x(1 - x)]^{1/2}S_{AB}$ for two different x values. Considering that only AB bonds are allowed, the closest distance between two tetrafunctional particles is about 2σ, showing up as a well-defined peak around π/σ. The B particles appear sharply coordinated with the A at distance σ (see the clear peak around $2\pi/\sigma$ in S_{AB}). Despite the tetrafunctional nature of the network formed by the A particles via the ABA bonds, no prepeak is observed in S_{AA}, a clear indication of a highly flexible and floppy network.[29] The network flexibility shows up also in the large value of the NN structure factor at the origin, a quantity related to the system compressibility.[30] Finally, we note that the large system size allows us to investigate in details the region $q\sigma < 2$, where all structure factors are close to their $q = 0$ limit.

BOND DYNAMICS

Figure 3 provides evidence of the reconfiguration of the network caused by the swapping events. The figure shows the normalized bond autocorrelation function $C_b(t)$ defined as

$$C_b(t) = \frac{n_b(t) - n_b(\infty)}{n_b(0) - n_b(\infty)} \quad (3)$$

where $n_b(t)$ is the fraction of bonds between pairs of particles which were present at time 0 and which are still present after time t. At infinite time, $n_b(\infty) = f_A/N_B$. Indeed, after an infinite time, each A particle has the same probability to be bonded to a B particle (the number of possible bonds between particles being N_AN_B). The f_AN_A bonds which were present at $t = 0$ can thus be still present at infinite time (after several breaking and forming events) with probability f_AN_A/N_AN_B simply for statistical reasons. The t dependence of $C_b(t)$ has a complex shape, which cannot be represented, for long times, with a single exponential. In particular, upon approaching zero, it develops an apparent power law with exponent around 1.5−2 whose precise characterization in terms of survival probability in the presence of multiple random walkers[31] would require much longer simulations. A meaningful typical decay time τ_b can be defined as $C_b(\tau_b) = 1/e$. τ_b, plotted as a function of $x_{fb} - x$ in Figure 3b, shows a clear inverse dependence on the total number of defects, diverging in the defect-free network with stoichiometric composition.

DOI: 10.1021/acs.macromol.7b02186
Macromolecules 2018, 51, 1232−1241

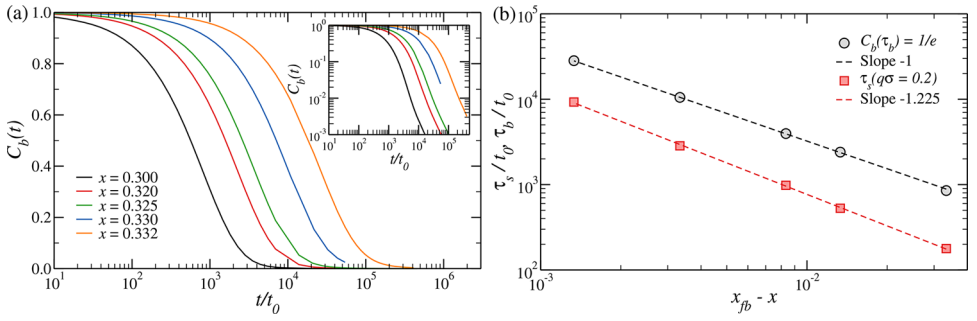

Figure 3. (a) Bond autocorrelation function $n_b(t)$ for different values of the concentration of A particles, x. (b) Dependence of the average bond lifetime on $x_{fb} - x$ in log−log scale. The same graph also shows the slow collective relaxation time τ_s also as a function of $x_{fb} - x$.

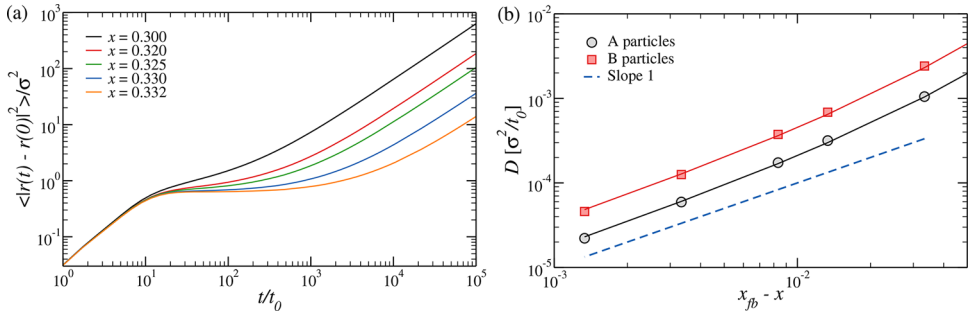

Figure 4. (a) Mean-square displacement of A particles. (b) Diffusion coefficient of the A and B particles as a function of $x_{fb} - x$. We recall here that the number of unreacted sites is $6N(x_{fb} - x)$.

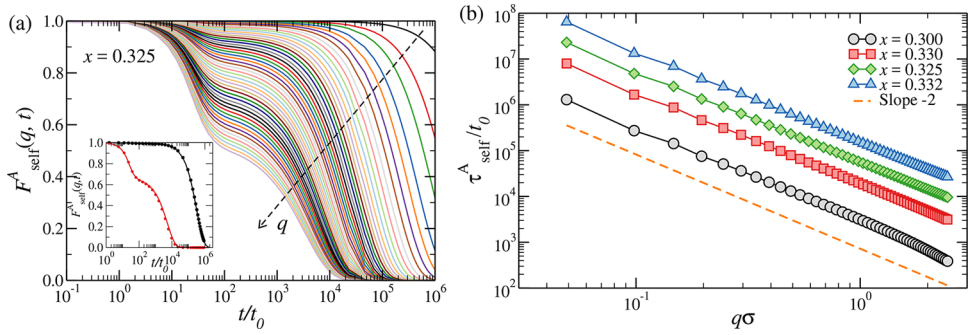

Figure 5. (a) Decay of $F_{self}(q,t)$ for the A particles ($F^A_{self}(q,t)$) for several q values ($0.05 < q\sigma < 2$) at $x = 0.325$, highlighting the two-step relaxation process. On decreasing q, the fast relaxation is progressively hidden and the plateau height approaches one. The inset compares for two different q values ($q\sigma = 0.24$ and $q\sigma = 1.92$) $F^A_{self}(q,t)$ (full lines) with the Gaussian approximation $\exp(-q^2\langle r^2(t)\rangle/6)$ (symbols), always for the A particles. (b) Wavevector dependence of the self-slow relaxation time $\tau^A_{self}(q)$ for the A particles.

TAGGED PARTICLE (SELF-)DYNAMICS

Mean-Square Displacement. The swap process is at the heart of the network reconfiguration. Both the single-particle (diffusion) and collective dynamics relaxations are slaved to the local changes in the network topology. The mean-square displacement of A particles for different values of the composition is reported in Figure 4a. The time dependence, as commonly featured in slow dynamics systems, can be separated in three parts: the very short time ballistic region, a subdiffusive regime signaled by a plateau, and the subsequent diffusive region. The plateau height is approximatively $0.64\sigma^2$ for the A particles. This quantity indicates the extent of particle displacement which can take place in the absence of bond-breaking processes. Its large value, compared to typical values of glass-forming liquids, marks one of the differences between open low-density gels and glasses. Indeed, in glasses the height of the plateau, controlled by excluded volume interactions, is of the order of $0.01\sigma^2$.[32] The diffusion coefficients, calculated from the long time limit of the mean-square displacement, are shown in Figure 4b as a function of $x_{fb} - x$. Both for A and B particles the diffusion coefficient can be well represented by the phenomenological expression

$$D = D_1(x_{fb} - x) + D_2(x_{fb} - x)^2 = [D_1 + D_2(x_{fb} - x)](x_{fb} - x) \quad (4)$$

This expression includes a linear term modeling the diffusion induced by the swapping of an isolated reactive site and a quadratic contribution arising from interactions between different reactive sites, which increases with $x_{fb} - x$. The right-hand side of eq 4 shows that the same functional form can also be interpreted as a diffusion process fully controlled by the number of reactive sites, diffusing across the network with a diffusion coefficient weakly dependent on their concentration.

DOI: 10.1021/acs.macromol.7b02186
Macromolecules 2018, 51, 1232−1241

Self-Dynamics. The self- (or tagged particle) dynamics is properly described in Fourier space by the q-dependent correlation functions

$$F_{\mathrm{self}}(\mathbf{q}, t) = \langle e^{i\mathbf{q}\cdot[\mathbf{r}_k(t)-\mathbf{r}_k(0)]}\rangle \quad (5)$$

where $\mathbf{r}_k(t)$ is the position of the generic k particle at time t. The average is over all particles of the same type and over distinct starting times. An additional average over different wavevectors with the same modulus can be performed by exploiting the isotropicity of the system. Figure 5a shows $F_{\mathrm{self}}(q,t)$ for the A particles ($F^A_{\mathrm{self}}(q,t)$) for several $q \equiv |\mathbf{q}|$ values for one x value. Similarly to the mean-square displacement, $F^A_{\mathrm{self}}(q,t)$ shows a two-step relaxation, associated with the decorrelation at fixed bonding and to the slow diffusive process. The time dependence can be accurately modeled by the functional form

$$F_{\mathrm{self}}(q, t) = Ae^{-t/\tau_{\mathrm{self},f}} + (1 - A)e^{-(t/\tau_{\mathrm{self},s})^{\beta}} \quad (6)$$

In the studied q range the stretching exponent β is always larger than 0.85 and approaches 1.0 on lowering q. The inset in Figure 5a compares $F^A_{\mathrm{self}}(q,t)$ and $\exp(-q^2\langle r^2(t)\rangle_A/6)$. The similarity between the two sets of curves for small q is consistent with the expected validity of the Gaussian approximation[26] and with the identification of the slow relaxation time $\tau^A_{\mathrm{self},s}$ with the diffusion time given by $(q^2D_A)^{-1}$. Similar results (not shown) hold also for the B particles and for all other x values.

COLLECTIVE DYNAMICS

The collective dynamics describes the way density fluctuations of different wavelengths evolve in the system. The normalized correlation function of the density fluctuations is defined as

$$F_{\mathrm{coll}}(\mathbf{q}, t) \equiv \frac{1}{S(\mathbf{q})}\left\langle \frac{1}{N}\sum_{kj} e^{i\mathbf{q}\cdot[\mathbf{r}_k(t)-\mathbf{r}_j(0)]}\right\rangle \quad (7)$$

where $S(\mathbf{q})$ is the structure factor, the average is again taken over different initial times, and the sum runs over all pairs of particles in the system, irrespective of their identity (NN). Analogous expressions can be written for the AA and BB components. Figure 6a compares for a specific small wavevector ($q\sigma = 0.15$) the self- and the collective correlation functions. Two observations are relevant: first of all, all partial correlation functions (AA, BB, and NN) decay on the same time scale, and hence in the following we will focus only on the NN correlation. Second, and more importantly, the self-autocorrelation function decays on a time scale much slower than the collective relaxation. This indicates that particle diffusion is not relevant for the decay of the collective density fluctuations at small wavevectors.

Figure 6b shows $F_{\mathrm{coll}}(q,t)$ for a generic x value and several q-vectors, in the region $q\sigma < 2$, where the structure factor is approximatively flat. For larger q, the local model-dependent structure becomes relevant, affecting the relaxation time. This large-q region has been extensively investigated in the case of glass-forming liquids.[33−37] The function shows a clear two-step relaxation, a fast decay associated with damped oscillations, and a slow decay that completes the memory loss process. Remarkably, here the slow-relaxation decay is identical, irrespective of the value of q. In all cases, $F_{\mathrm{coll}}(\mathbf{q},t)$ can be very accurately modeled by a damped harmonic oscillator correlation function

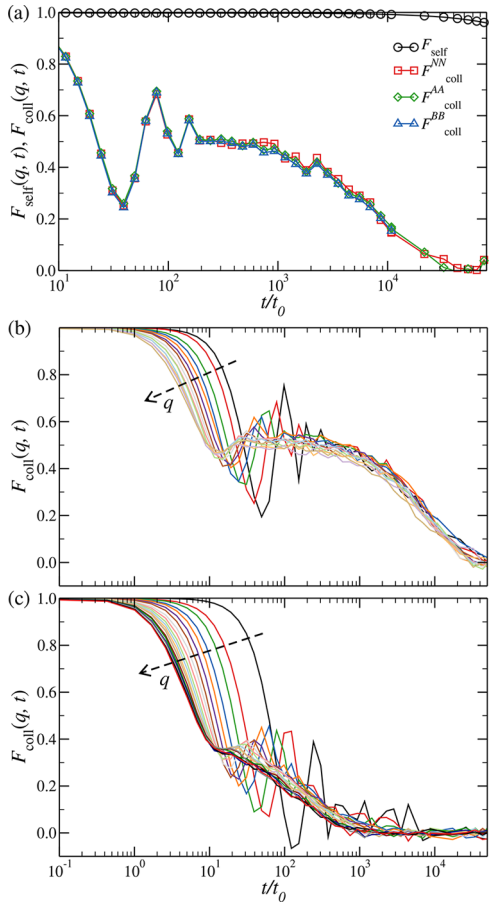

Figure 6. (a) Comparison between self- and collective decays for $x = 0.332$ and $q\sigma = 0.15$. (b) Decay of $F_{\mathrm{coll}}(q,t)$ for $0.04 \le q\sigma \le 2$ at $x = 0.332$, highlighting the two-step relaxation process. (c) Decay of $F_{\mathrm{coll}}(q,t)$ for $0.04 \le q\sigma \le 2$ at $x = 0.300$. Note how the q-dependent damped sound almost takes over the α relaxation mode at the smallest investigated q.

$$F_{\mathrm{coll}}(q, t) = Ae^{-t/\tau_f}\cos(\Omega t) + (1 - A)e^{-(t/\tau_s)^{\beta}} \quad (8)$$

where A and $(1 - A)$ are respectively the amplitude of the fast and slow relaxation processes, with associated time scales τ_f and τ_s. The angular frequency Ω accounts for the propagation phenomenon described by the fast relaxation. The slow process is modeled via a stretched exponential function, with a stretching exponent β to account for the variety of relaxation times characterizing disordered systems. All fitting parameters (A, τ_f, τ_s, Ω, and β) depend, in principle, on q.

An example of the quality of the fit is shown in Figure 7a. The fit allows us to extract the sound dispersion relation Ω vs q (Figure 7b) and the damping of the sound mode $1/\tau_f$. The q dependence of Ω at small q is consistent with a sound speed of 0.53 ± 0.03 $[\sigma/t_0]$. Interestingly, while the fast decay time follows a q dependence that approaches at small q the expected q^{-2} behavior, the slow decay time is essentially wavevector independent. This feature, already very evident in the shape of the correlation function reported in Figure 6b, is highlighted in Figure 7c, which reports τ_s and τ_f vs q for all investigated x.

First of all, the fact that the fast dynamics remains constant even for $x \to x_{fb}$ shows that it can be associated without ambiguity to the vibrational dynamics of the permanent network of bonds. Second, the fast relaxation time τ_f and Ω do not significantly depend on the fraction of reactive sites for

DOI: 10.1021/acs.macromol.7b02186
Macromolecules 2018, 51, 1232−1241

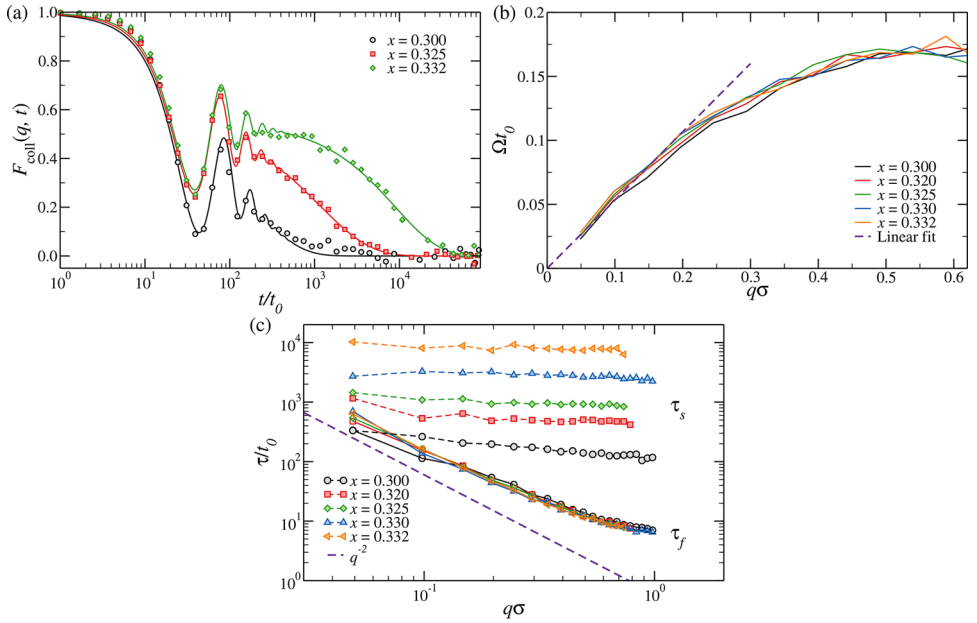

Figure 7. (a) Collective density correlation function for $q\sigma = 0.146$ at $x = 0.300$, $x = 0.325$, and $x = 0.332$ and the corresponding fit according to eq 8. (b) Ω vs q as resulting from the fit. (c) Wavevector dependence of the collective fast $\tau_f(q)$ and slow relaxation times $\tau_s(q)$.

the range of x considered here. This can be rationalizing by considering that according to the Newton−Laplace equation, the speed of sound (at small q) can be written as $\Omega = (K/\rho)^{1/2}$, where K is the bulk modulus of the material. Since all investigated systems have the same density ($\rho\sigma^3 = 0.38$), the only possible source of x dependence is K, which in amorphous solids is linked to the total number of bonds.[38−40] The fact that for the systems considered here this number does not change by more than ≈10% explains the weak dependence of Ω on x.

The first decay of the correlation function, of amplitude A, results from the decorrelation process induced by the vibrational dynamics (the normal modes of the network). This process is significantly faster than the slow process (of amplitude $1 - A$) at large q, but it becomes comparable in time (due to the different q dependence of τ_s and τ_f) at very small q. Indeed, the fact that τ_s is q-independent determines the presence of a crossover wavevector q_c at which the network restructuring takes place on a time scale comparable with the vibrational process. Figure 6c provides an illustration of such a case. For much smaller wavevectors, $q \ll q_c$, the vibrational dynamics does not take place any longer on a network with static links but on a "homogeneous" sample for which the memory of the original network links has been completely washed out. Only below q_c are hydrodynamic predictions expected to properly model the decay of the density fluctuations in the system.

To identify the reasons behind the q^0 behavior of τ_s, we investigate the dependence of τ_s on x. We report the data in two different ways. First, we show in Figure 3 τ_s vs $x_{fb} - x$ at one small q. The comparison with the bond characteristic lifetime shows that the latter is always at least a factor of 2 larger than τ_s. Therefore, the length scale-invariant relaxation of the density fluctuations we observe does not require the swapping of all networks bonds. In fact, only a fraction of all bonds need to swap in order to relax the density. Moreover, the dependence of τ_s on the number of reactive sites differs from the one of τ_b. Indeed, while the former is well described by a power-law with exponent ≈ −1.2, the latter behaves as $1/(x_{fb} - x)$. Thus, even though the two time scales are clearly connected (both being linked to the restructuring of the network) their mutual relation is not straightforward.

Figure 8 shows instead τ_s normalized by the diffusion coefficient of the B particles (D_B) to account for the efficiency

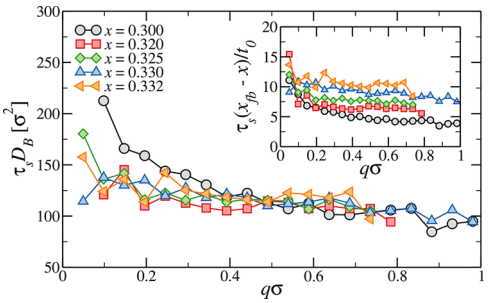

Figure 8. Scaling behavior of the slow relaxation time. The main panel shows the good collapse of the curves obtained by multiplying τ_s by D_B for all but the lowest values of x. The inset shows that multiplication of τ_s by $(x_{fb} - x)$ is not sufficient to obtain a proper scaling.

of the swapping process. As shown in the inset of Figure 8, the bare number of reactive sites is not a perfect scaling variable, but it is indeed necessary to incorporate the minor x dependence of the swapping time (see eq 4). The quality of the scaling of the data shown in the main figure for different x confirms indeed that the time scale of the swapping process fully accounts for the slow relaxation process.

To grasp why the rearrangement of the network topology through the diffusive motion of the reactive sites gives rise to a decay of the density fluctuations that takes place on the same time scale for all lengths, we refer to a recently proposed simple model.[23] In ref 23 each independent region of the system (e.g., a region of size larger than any static correlation length) is considered to be a point particle of fixed mass (the bead) attached to its neighboring regions via an elastic constant (the spring) which can fluctuate between different values. The different elastic constant values mimic the different local

DOI: 10.1021/acs.macromol.7b02186
Macromolecules 2018, 51, 1232−1241

elasticity associated with the different local bonding pattern. The system is thus modeled as a one-dimensional chain composed of beads and springs in the presence of a thermal bath which induces a viscous damping and exerts random forces on each bead. The resulting equation of motion in the overdamped limit is thus

$$-k_n(u_n - u_{n-1} - l_0) + k_{n+1}(u_{n+1} - u_n - l_0) - \gamma\frac{du_n}{dt} + f_n = 0 \quad (9)$$

where u_n is the position of bead n, k_n is the elastic constant acting between beads n and $n + 1$, l_0 is the equilibrium distance, γ is the viscous damping on the beads, and f_n is the delta-correlated random force acting on bead n, whose amplitude is fixed by the dissipation−fluctuation theorem. Periodic boundary conditions are also assumed. When the elastic constants are equal (e.g., $k_n = K$ for all n), eq 9 shows that the density fluctuations relax with a time $\tau = (\gamma/K)(ql_0)^{-2}$ which grows with q^{-2}, the typical dependence of the dispersion relation in colloidal crystals. To introduce in the model the possibility that the local elastic constant changes due to the intervention of swap processes which alter the network connectivity, one can assume that each k_n can independently fluctuate between two different equiprobable values K_1 and K_2. The autocorrelation time of the spring value can be described assuming a simple Markov process as

$$\langle k_n(t)k_n(0)\rangle = \left(\frac{K_1 - K_2}{2}\right)^2 \exp(-t/\tau_s) + \left(\frac{K_1 + K_2}{2}\right)^2 \quad (10)$$

where τ_s indicates here the average time between changes in the k_n values.

A change in the elastic constant brings in a change in the local density which propagates with the fast damped oscillation motion, providing the channel for density decorrelation. The numerical solution of this model[23] shows in this case the presence of two relaxation processes: a process with a q^{-2} dependence (the same observed in the case of identical springs) and an additional process with a time scale controlled by τ_s, i.e., the time required by a spring to lose memory of its initial value. Thus, under the assumption that particle diffusion (not included in the model) is not relevant for relaxing the density fluctuations and for length scales larger than any spatial correlation length in the system (such that independent relaxing units can be defined), this model predicts a wavevector-independent α-relaxation process. In the system studied here (and in ref 23), the time scale associated with the restructuring of the network plays the role of the characteristic time of the local springs, and it is fully controlled by the rate of the bond-swapping process, which therefore sets the overall relaxation time. For large length scales, the system can be thus imagined as a composition of independently relaxing units, all of them forgetting their original state with the same time τ_s. As a result, the local nature of the relaxation process and the absence of any correlation between the relaxation of the independent units are at the heart of the q^0 behavior. The q^0 process would not be observed if the relaxation of the single unit would require for example a relaxation of the particle relative composition, which would then impose, by virtue of particle conservation, a diffusive contribution to the relaxation consistent with the mode-coupling predictions for binary systems.[41,42]

The simple model introduced above can be easily generalized by considering a continuous distribution of spring constants of finite variance. Indeed, these can be considered as proxies for the varying elasticity, which in turn is connected to the network topology of the local relaxing units. A sketch of the basic physical idea behind the model is shown in Figure 9.

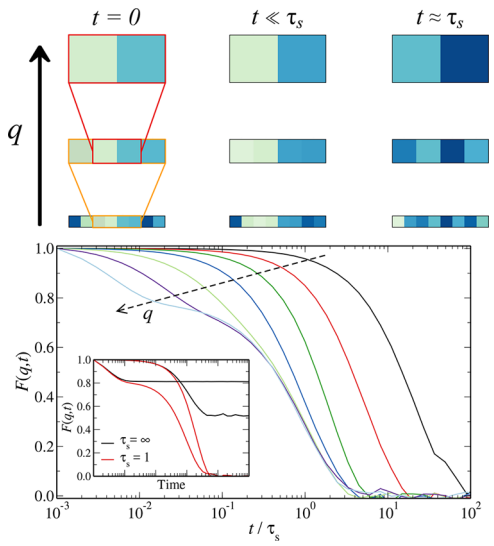

Figure 9. (a) The sketch represents a collection of independently relaxing units (small squares), whose size is larger than the static correlation length. The different colors indicate the different values of the local elastic constant, which fluctuate in time, according to the microscopic dynamics provided by the bond-swapping process. Only when the elapsed time is of the order of τ_s is the local elastic constant uncorrelated with the value at time zero. The horizontal direction indicates the time evolution, and the vertical direction indicates the length scale probed by different wavevectors q (progressively enlarging the field of view). The relaxation of the elastic constant over any length scale requires the decorrelation of all its independent subunits, a time which is always equal to τ_s. (b) Collective decay of the density fluctuations for the model (eqs 9 and 10) when $\tau_s = 1$. Curves for $ql_0 =$ 1, 2, 4, 8, 16, 32, and 64 are shown. For $ql_0 \gtrsim 10$, two relaxation processes are observed: one q-dependent linked to the vibrational dynamics and one q-independent associated with the spring relaxation process. In the inset, a comparison between relaxing and nonrelaxing springs is reported for $ql_0 = 4$ and $ql_0 = 40$.

Finally, we note that the occurrence of a q-independent relaxation time results from the solution of mode-coupling equations for one-component liquids in the small wavevector region[41] when only density and current fluctuations are included in the theoretical description. This q^0 behavior has been linked to a conservation law.[42] Indeed, the occurrence of a q^0 mode in one-component systems has been ascribed to the existence of a conserved quantity (the number of particles) that is associated with a flux that is also conserved (the overall momentum). By contrast, in mixtures momentum is not conserved at the single-species level,[42] since there is interspecies momentum exchange. The present system sits somewhat in the middle, since it is a binary mixture (and thus should not exhibit a q^0 behavior according to the above argument), but concentration fluctuations are greatly suppressed by the nearly stoichiometric conditions and by the fact that bonding is allowed between unlike species only. Unfortunately, our results cannot reliably corroborate nor rule out the possibility that the q^0 behavior observed here is

DOI: 10.1021/acs.macromol.7b02186
Macromolecules 2018, 51, 1232−1241

directly connected to momentum conservation on an intermediate length scale.

SUMMARY AND CONCLUSIONS

We have investigated, via molecular dynamics simulations, the self-dynamics and collective dynamics in a nonstoichiometric binary network in its fully bonded configuration. Specifically, we have studied the experimentally relevant case[1] in which tetravalent particles (A) are mixed in excess of bivalent particles (B) such that in the fully bonded condition an excess of unbounded B-sites exist. When the thermal vibration of the network brings one of these unreacted site geometrically close to an existing AB bond, a swap process takes place which allows for network restructuring. The implementation of the recently proposed swap algorithm[22] makes it possible to perform molecular dynamics simulations which mimic exchange reactions.

By simulating very large systems for very long times, exploiting the computational power of graphic processing units with a homemade code, we have been able to access very small wavevectors, comparable to the one probed in light scattering experiments (corresponding to wavelengths of up to 100 times the nearest-neighbor distance). We have found that in this small q region the collective density fluctuations decay with a two-step process. The fast process is associated with the damped elastic motion of the system at fixed bonding pattern. The slow process is associated with the restructuring of the bond network, mediated by a sequence of elementary bond-switch processes. Interestingly, a single time scale controls the decay of the slow density fluctuations at all investigated wavevectors. A wavevector-independent collective relaxation has been previously reported in some soft-matter systems, including rodlike micelles,[43] in solutions of telechelic ionomers in toluene reversibly connected by the association of their ionic terminal groups,[44] in water-soluble polymers with hydrophobic end blocks acting as bridges between different droplets,[24] and in polymer melts.[45,46] Recent simulations of a highly directional tetrahedral network also reported indications of a q^0 mode, but the limited system size did not allow for a proper determination of the small wavevector behavior.[47]

Theoretical models based on memory functions[48] in which the decay of the memory is assumed to be independent of the wavevector have been in the past used to interpret the aforementioned experimental results. Mode coupling theory,[41] in the limit of very small wavevector, also predicts a wavevector-independent memory function and a q^0 mode. Hence we speculate that the q^0 behavior should be shared by all systems composed by independently relaxing distinct regions in the region of wavelengths larger than the characteristic size of the relaxing units, if particle diffusion is not relevant. Finally, our results also suggest that vitrimeric systems, in which the bond-switching mechanism is at the heart of the network reconfiguration, should have in the q^0 mode their characteristic signature.

APPENDIX. THE BOND-SWAPPING ALGORITHM

For the sake of completeness, we review here the method introduced in ref 22 to implement a bond-swapping mechanism in molecular dynamics simulations.

We assume that the system is composed by two type of particles (A and B), with each having a number of interacting sites providing the particle functionality (or valence). Sites of unlike species interact through a bonding potential (eq 2 and Figure 1d). In a swap process, when an unreacted site of a particle finds itself close to a bonded pair, it gives rise to an activated complex which then decays again in a bonded pair and an isolated unreacted site. The swap is successful if the incoming particle replaces the originally bonded particle of the same type. This can be schematized with the reactions

$$A_iB_k + B_j = A_iB_j + B_k \quad \text{or} \quad A_kB_i + A_j = A_jB_i + A_k \tag{11}$$

where A_j indicates the j site of a type A particle and analogously B_k indicates the k site of a type B particle.

An effective computational algorithm must fulfill two conditions: (i) Each site should not be able to form more than two bonds. Indeed, each site should be bonded with two other sites only during the swap process. This is a necessary condition to model particles with well-defined functionalities. (ii) It must be possible to control the activation energy of the swap process. It should be possible to tune the activation energy from infinity (no swap processes, only bond breaking and re-forming) to zero (no energetic cost for swapping).

To fulfill the two previous conditions, the method introduced in ref 22 suggests to complement the two-body interaction with a three-body potential V_{3b} that acts between all triplets of bonded sites (either ABA or BAB). Indicating with r_{ss}^{ij} and r_{ss}^{ik} the distances between sites i and j and i and k, the three-body contribution reads

$$V_{3b}(r_{ss}^{ij}, r_{ss}^{ik}) = \lambda\epsilon V_3(r_{ss}^{ij})V_3(r_{ss}^{ik}) \tag{12}$$

with

$$V_3(r) = \begin{cases} 1 & \text{for } r \le \sigma_{ss} \\ -\dfrac{V_{ss}(r)}{|\epsilon|} & \text{for } \sigma_{ss} < r < r_c \end{cases} \tag{13}$$

where λ is a parameter controlling the activation energy, ϵ is the depth of the two-body bonding potential, σ_{ss} is the optimal bonding distance (the position of the minimum in the bonding potential in eq 2), and r_c is the cutoff distance in the same bonding potential. Note that since $V_{ss}(r)$ is always negative for $r > \sigma_{ss}$, V_3 is always positive. Thus, the sign of the three-body contribution is controlled by the sign of λ.

To grasp how the method works, we use the notation of eq 11 (left) and consider how the potential energy changes when an unreacted site B_j moves to a distance $r < r_c$ from A_i, the site involved in the A_iB_k bond. Since the bonding interaction involves only distinct pairs, only the A_i site is involved in two interactions, and hence only one single triplet needs to be considered ($B_jA_iB_k$). The potential energy of these three particles is thus given by the sum of the pair interaction energy between B_j and A_i, the pair interaction energy between B_k and A_i, and the triplet interaction energy between B_j, A_i, and B_k. Assuming the limiting case in which both B_jA_i and B_kA_i are at the optimal distance σ_{ss}, then $V_{ss} = -\epsilon$ and $V_{3b} = \lambda\epsilon$. As a result, the total potential energy is $-2\epsilon + \lambda\epsilon$. If $\lambda = 1$, then the additional gain of forming one more bond is exactly compensated by the three-body contribution: the swap process does not require any energetic cost. On increasing λ, the formation of a triplet becomes energetically expensive, providing the possibility of encoding the presence of an activation barrier.

DOI: 10.1021/acs.macromol.7b02186
Macromolecules 2018, 51, 1232−1241

The three-body potential helps also avoiding the formation of multiply bonded sites. Indeed, if three B interacting sites are close to one A site, then the bonding potential contributes about -3ϵ. However, the three-body potential gives $+3\lambda\epsilon$ (since there are now three possible triplets), generating a configuration with a significantly higher potential energy than a bonded pair.

The swap method thus requires $\lambda \geq 1$. For $\lambda = 1$ the swap dynamics is most effective, and the restructuring of the bond network is not hindered. By contrast, values of $\lambda > 1$ allow to simulate the effect of an activation energy on the swap process.

AUTHOR INFORMATION

Corresponding Author

*E-mail: lorenzo.rovigatti@gmail.com (L.R.).

ORCID

Lorenzo Rovigatti: 0000-0001-5017-2829

Tommaso Bellini: 0000-0003-4898-4400

Notes

The authors declare no competing financial interest.

ACKNOWLEDGMENTS

We thank T. Voigtmann and E. Zaccarelli for fruitful discussions.

REFERENCES

(1) Montarnal, D.; Capelot, M.; Tournilhac, F.; Leibler, L. Silica-like malleable materials from permanent organic networks. *Science* **2011**, *334*, 965−968.

(2) Kloxin, C. J.; Bowman, C. N. Covalent adaptable networks: smart, reconfigurable and responsive network systems. *Chem. Soc. Rev.* **2013**, *42*, 7161−7173.

(3) Denissen, W.; Winne, J. M.; Du Prez, F. E. Vitrimers: permanent organic networks with glass-like fluidity. *Chemical Science* **2016**, *7*, 30−38.

(4) Capelot, M.; Unterlass, M. M.; Tournilhac, F.; Leibler, L. Catalytic control of the vitrimer glass transition. *ACS Macro Lett.* **2012**, *1*, 789−792.

(5) Denissen, W.; Rivero, G.; Nicolaÿ, R.; Leibler, L.; Winne, J. M.; Du Prez, F. E. Vinylogous urethane vitrimers. *Adv. Funct. Mater.* **2015**, *25*, 2451−2457.

(6) Angell, C. A. Formation of Glasses From Liquids and Biopolymers. *Science* **1995**, *267*, 1924−1935.

(7) Lu, Y.-X.; Tournilhac, F.; Leibler, L.; Guan, Z. Making Insoluble Polymer Networks Malleable via Olefin Metathesis. *J. Am. Chem. Soc.* **2012**, *134*, 8424−8427.

(8) Zheng, P.; McCarthy, T. J. A Surprise from 1954: Siloxane Equilibration Is a Simple, Robust, and Obvious Polymer Self-Healing Mechanism. *J. Am. Chem. Soc.* **2012**, *134*, 2024−2027.

(9) Rubinstein, M.; Colby, R. H. *Polymer Physics*; Oxford University Press: New York, 2003; Vol. *23*.

(10) Tanaka, F. *Polymer Physics: Applications to Molecular Association and Thermoreversible Gelation*; Cambridge University Press: 2011.

(11) Wittmer, J. P.; Kriuchevskyi, I.; Cavallo, A.; Xu, H.; Baschnagel, J. Shear-stress fluctuations in self-assembled transient elastic networks. *Phys. Rev. E: Stat. Phys., Plasmas, Fluids, Relat. Interdiscip. Top.* **2016**, *93*, 062611.

(12) Kriuchevskyi, I.; Wittmer, J.; Benzerara, O.; Meyer, H.; Baschnagel, J. Numerical determination of shear stress relaxation modulus of polymer glasses. *Eur. Phys. J. E: Soft Matter Biol. Phys.* **2017**, *40*, 43.

(13) Biffi, S.; Cerbino, R.; Bomboi, F.; Paraboschi, E. M.; Asselta, R.; Sciortino, F.; Bellini, T. Phase behavior and critical activated dynamics of limited-valence DNA nanostars. *Proc. Natl. Acad. Sci. U. S. A.* **2013**, *110*, 15633−15637.

(14) Biffi, S.; Cerbino, R.; Nava, G.; Bomboi, F.; Sciortino, F.; Bellini, T. Equilibrium gels of low-valence DNA nanostars: a colloidal model for strong glass formers. *Soft Matter* **2015**, *11*, 3132−3138.

(15) Bomboi, F.; Biffi, S.; Cerbino, R.; Bellini, T.; Bordi, F.; Sciortino, F. Equilibrium gels of trivalent DNA-nanostars: Effect of the ionic strength on the dynamics. *Eur. Phys. J. E: Soft Matter Biol. Phys.* **2015**, *38*, 1−8.

(16) Bomboi, F.; Romano, F.; Leo, M.; Fernandez-Castanon, J.; Cerbino, R.; Bellini, T.; Bordi, F.; Filetici, P.; Sciortino, F. Re-entrant DNA gels. *Nat. Commun.* **2016**, *7*, 13191.

(17) Smallenburg, F.; Leibler, L.; Sciortino, F. Patchy particle model for vitrimers. *Phys. Rev. Lett.* **2013**, *111*, 188002.

(18) Wertheim, M. S. Fluids with highly directional attractive forces. I. Statistical thermodynamics. *J. Stat. Phys.* **1984**, *35*, 19.

(19) Wertheim, M. S. Fluids with highly directional attractive forces. II. Thermodynamic perturbation theory and integral equations. *J. Stat. Phys.* **1984**, *35*, 35−47.

(20) Long, R.; Qi, H. J.; Dunn, M. L. Modeling the mechanics of covalently adaptable polymer networks with temperature-dependent bond exchange reactions. *Soft Matter* **2013**, *9*, 4083−4096.

(21) Meng, F.; Pritchard, R. H.; Terentjev, E. M. Stress Relaxation, Dynamics, and Plasticity of Transient Polymer Networks. *Macromolecules* **2016**, *49*, 2843−2852.

(22) Sciortino, F. Three-body potential for simulating bond swaps in molecular dynamics. *Eur. Phys. J. E: Soft Matter Biol. Phys.* **2017**, *40*, 3.

(23) Nava, G.; Rossi, M.; Biffi, S.; Sciortino, F.; Bellini, T. The fluctuating elasticity mode in transient molecular networks. *Phys. Rev. Lett.* **2017**, *119*, 078002.

(24) Michel, E.; Filali, M.; Aznar, R.; Porte, G.; Appell, J. Percolation in a Model Transient Network: Rheology and Dynamic Light Scattering. *Langmuir* **2000**, *16*, 8702−8711.

(25) Stockmayer, W. H. Molecular distribution in condensation polymers. *J. Polym. Sci.* **1952**, *9*, 69−71.

(26) Hansen, J.-P.; McDonald, I. R. *Theory of Simple Liquids*; Elsevier: 1990.

(27) Stillinger, F. H.; Weber, T. A. Computer simulation of local order in condensed phases of silicon. *Phys. Rev. B: Condens. Matter Mater. Phys.* **1985**, *31*, 5262.

(28) Russo, J.; Tartaglia, P.; Sciortino, F. Reversible gels of patchy particles: Role of the valence. *J. Chem. Phys.* **2009**, *131*, 014504.

(29) Saika-Voivod, I.; Smallenburg, F.; Sciortino, F. Understanding tetrahedral liquids through patchy colloids. *J. Chem. Phys.* **2013**, *139*, 234901.

(30) Barrat, J. L.; Hansen, J. P. *Basic Concepts for Simple and Complex Fluids*; Cambridge University Press: 2003.

(31) Redner, S. *A Guide to First-Passage Processes*; Cambridge University Press: 2001.

(32) Binder, K.; Kob, W. *Glassy Materials and Disordered Solids: An Introduction to Their Statistical Mechanics*; World Scientific: 2011.

(33) Horbach, J.; Kob, W. Relaxation dynamics of a viscous silica melt: The intermediate scattering functions. *Phys. Rev. E: Stat. Phys., Plasmas, Fluids, Relat. Interdiscip. Top.* **2001**, *64*, 041503.

(34) Kob, W.; Andersen, H. C. Testing mode-coupling theory for a supercooled binary Lennard-Jones mixture. II. Intermediate scattering function and dynamic susceptibility. *Phys. Rev. E: Stat. Phys., Plasmas, Fluids, Relat. Interdiscip. Top.* **1995**, *52*, 4134−4153.

(35) Sciortino, F.; Fabbian, L.; Chen, S.-H.; Tartaglia, P. Supercooled water and the kinetic glass transition. II. Collective dynamics. *Phys. Rev. E: Stat. Phys., Plasmas, Fluids, Relat. Interdiscip. Top.* **1997**, *56*, 5397.

(36) Chong, S.-H.; Sciortino, F. Structural relaxation in supercooled orthoterphenyl. *Phys. Rev. E* **2004**, *69*, 051202.

(37) Bhattacharyya, S. M.; Bagchi, B.; Wolynes, P. G. Facilitation, complexity growth, mode coupling, and activated dynamics in supercooled liquids. *Proc. Natl. Acad. Sci. U. S. A.* **2008**, *105*, 16077−16082.

(38) Zaccone, A. Elastic Deformations in Covalent Amorphous Solids. *Mod. Phys. Lett. B* **2013**, *27*, 1330002.

DOI: 10.1021/acs.macromol.7b02186
Macromolecules 2018, 51, 1232−1241

(39) Zaccone, A.; Scossa-Romano, E. Approximate analytical description of the nonaffine response of amorphous solids. *Phys. Rev. B: Condens. Matter Mater. Phys.* **2011**, *83*, 184205.
(40) Huisman, E. M.; Lubensky, T. C. Internal Stresses, Normal Modes, and Nonaffinity in Three-Dimensional Biopolymer Networks. *Phys. Rev. Lett.* **2011**, *106*, 088301.
(41) Götze, W. *Complex Dynamics of Glass-Forming Liquids: A Mode-Coupling Theory*; OUP: Oxford, 2008; Vol. *143*.
(42) Weysser, F.; Puertas, A. M.; Fuchs, M.; Voigtmann, T. Structural relaxation of polydisperse hard spheres: Comparison of the mode-coupling theory to a Langevin dynamics simulation. *Phys. Rev. E* **2010**, *82*, 011504.
(43) Nemoto, N.; Kuwahara, M.; Yao, M.-L.; Osaki, K. Dynamic light scattering of CTAB/NaSal threadlike micelles in a semidilute regime. 3. Dynamic coupling between concentration fluctuation and stress. *Langmuir* **1995**, *11*, 30−36.
(44) Johannsson, R.; Chassenieux, C.; Durand, D.; Nicolai, T.; Vanhoorne, P.; Jerome, R. Dynamic properties of the transient network formed by telechelic ionomers studied by dynamic light scattering and dynamic mechanical analysis. *Macromolecules* **1995**, *28*, 8504−8510.
(45) Adam, M.; Delsanti, M. Dynamical behavior of semidilute polymer solutions in a. THETA. solvent: quasi-elastic light scattering experiments. *Macromolecules* **1985**, *18*, 1760−1770.
(46) Li, J.; Ngai, T.; Wu, C. The slow relaxation mode: from solutions to gel networks. *Polym. J.* **2010**, *42*, 609−625.
(47) Roldán-Vargas, S.; Rovigatti, L.; Sciortino, F. Connectivity, dynamics, and structure in a tetrahedral network liquid. *Soft Matter* **2017**, *13*, 514−530.
(48) Brochard, F. Gel-like modes. of polymer solutions in $\ll \theta \gg$ solvents. *J. Phys. (Paris)* **1983**, *44*, 39−43.

DOI: 10.1021/acs.macromol.7b02186
Macromolecules 2018, 51, 1232−1241